Proceedings of the 35th European Safety and Reliability & the 33rd Society for Risk Analysis Europe Conference
Edited by Eirik Bjorheim Abrahamsen, Terje Aven, Frederic Bouder, Roger Flage, Marja Ylönen
 Published by Research Publishing, Singapore.
doi: 10.3850/978-981-94-3281-3_ESREL-SRA-E2025-P1242-cd

Research on Phase Transition and Flow Characteristics of Tubing Leakage in CO_2 Injection Wells

Zhiming Jiang

College of Safety and Ocean Engineering, China University of Petroleum-Beijing/Key Laboratory of Oil and Gas Safety and Emergency Technology, Ministry of Emergency Management, China. E-mail: jzm_cup@163.com

Jianchun Fan

College of Safety and Ocean Engineering, China University of Petroleum-Beijing/Key Laboratory of Oil and Gas Safety and Emergency Technology, Ministry of Emergency Management, China. E-mail: fjc688@126.com

Over the past decade, with the increasing number and scale of Carbon Capture and Storage (CCS) projects internationally, the integrity of CO_2 injection wells has brought growing concern. The downhole tubing is highly susceptible to corrosion and perforation due to factors such as high-pressure low-temperature injection and CO_2 corrosion, which can subsequently lead to wellbore integrity failure. This study employs the Computational Fluid Dynamics (CFD) software Fluent to establish a CFD model for investigating the leakage flow characteristics of downhole tubing in CO_2 injection wells. This model incorporates NIST-based CO_2 property equations, which accurately capture the depressurization phase transition and gas-liquid coexistence phenomena during the leakage process. By studying the flow characteristics of tubing leakage in CO_2 injection wells, this paper reveals the variation patterns of temperature, pressure, and flow velocity during the transient leakage process. The research findings provide a foundation for understanding the flow characteristics of tubing leakage in CO_2 injection wells, supporting the safe and long-term effective operation of CCS projects.

Keywords: CO_2 injection wells, Tubing leakage, Phase transition, Leakage hole diameter, Integrity of CO_2 injection wells, Flow characteristics.

1 Introduction

Over the past decade, the number and scale of carbon capture and storage (CCS) projects have been expanding internationally. As of July 31, 2023, publicly disclosed CCS projects in the development, construction, and operational stages have reached a total carbon dioxide capture capacity of 361 million tons per annum (Mtpa), representing an increase of nearly 50% compared to the data in the 2022 Global CCS Status Report. In the entire process, carbon storage is the crucial link to ensure the long-term safe storage of captured carbon dioxide, directly impacting the actual emission reduction effectiveness of CCS technology. In the event of an accident (Xi and Lu et al. 2023), it may cause significant damage to the surrounding soil environment, endanger human health and safety, lead to socio-economic losses, and exacerbate the greenhouse effect. The integrity of CO_2 injection wells has been receiving increasing attention. Due to high-pressure low-temperature injection and CO_2 corrosion, downhole tubing is prone to corrosion and perforation (Peng and Lu et al. 2024), leading to wellbore integrity failure.

There has been limited simulation research on the leakage of downhole tubing in CO_2 injection wells by domestic and international scholars. In

recent years, many researchers have conducted extensive studies on near-field CO_2 leakage through simulations, achieving significant results. Liu developed a CFD model for simulating near-field leakage of high-pressure CO_2 pipelines, using the PR equation of state to assume CO_2 as a homogeneous medium without considering phase change during the near-field leakage process (Liu and Godbole et al. 2014). Elshahomi embedded a UDF program based on the GERG(General Equation of State for Gases)-2008 equation of state into a Fluent model to predict the decompression wave speed characteristics inside the pipeline due to high-pressure CO_2 leakage (Elshahomi and Lu et al. 2015). Liu further developed Elshahomi's model by introducing mass transfer and latent heat source terms into the UDF code to simulate the phase change process from nonequilibrium liquid to vapor and discussed the impact of impurities in CO_2 pipelines on decompression wave speed (Liu and Liu et al. 2018). Flechas used Fluent to compare the applicability of the Peng-Robinson and Span-Wagner equations of state in a two-dimensional full-bore fracture decompression model, considering nonequilibrium phase change and metastable liquid properties to simulate the transient decompression process of pure liquefied CO_2 pipelines (Flechas and Laboureur et al. 2020). Teng established a compressible phase change model considering real gas behavior of CO_2 based on the homogeneous relaxation model (HRM) to predict near-field CO_2 leakage (Teng and Liu et al. 2020). (Luo and Wu et al. 2024) Luo developed a near-field CO_2 leakage model considering dry ice formation, with the size distribution of dry ice particles described by the Rosin-Rammler expression, and studied the influence of different parameters on the safety distance of near-field CO_2 leakage.

Simultaneously, domestic and international scholars have also conducted research on flow noise. Zhu modeled the subsonic jet problem of jet aircraft, demonstrating the capability of large eddy simulation solvers based on unstructured grids to accurately simulate both cold and hot jet noise phenomena (Zhu and Pérez Arroyo et al. 2018). Wei conducted simulation studies on noise reduction for supersonic jets by step corrections at the nozzle trailing edge, capturing the far-field acoustic results of two different stepped nozzles under two under-expanded conditions. Traditionally, pipeline leak detection relies on semi-empirical formulas (Wei and Mariani et al. 2019). Zhang conducted experimental and simulation studies on the acoustic characteristics of natural gas pipeline leakage and found that natural gas pipeline leakage is a broadband noise mainly concentrated below 20 Hz, with the average sound pressure increasing with internal pressure and leak diameter (Zhang and Lian et al. 2021). Chen investigated the characteristics of heated transitional supersonic jets ejected from rectangular nozzles under overexpanded conditions using large eddy simulation and the Ffowcs-Williams and Hawkings acoustic analogy method. The results showed that as the temperature increased, jet speed significantly increased, and high-temperature jets exhibited antisymmetric oscillation mode characteristics at screech frequencies (Chen and Gojon et al. 2021). Cheng proposed a novel numerical model to analyze the noise distribution pattern of elliptical holes (Cheng and Zhang et al. 2024). First, the gas leakage flow field was solved using the large eddy simulation method, and then the near-field noise distribution was calculated. The velocity distribution pattern of elliptical jets was used as an analogy, leading to the velocity distribution function of elliptical defect boundaries. The model found that, with an increasing aspect ratio, the sound pressure level reduction rate along the minor axis exceeded that along the major axis.

This study employs the Computational Fluid Dynamics (CFD) software Fluent to establish a CFD model for investigating the leakage flow characteristics of downhole tubing in CO_2 injection wells. This model incorporates NIST-based CO_2 property equations, which accurately capture the depressurization phase transition and gas-liquid coexistence phenomena during the leakage process. By studying the flow characteristics of tubing leakage in CO_2 injection wells, this paper reveals the variation patterns of temperature, pressure, and flow velocity during the transient leakage process. The research findings provide a foundation for understanding the flow characteristics of tubing leakage in CO_2 injection wells, supporting the safe and long-term effective operation of CCS projects.

2 Simulation method

2.1 *Physical Process of Downhole Tubing Leakage*

As shown in Figure 1, this study simplifies the physical model of CO_2 injection well downhole tubing leakage, focusing on the local area of the leakage hole. The main focus is on the physical process of high-pressure CO_2 leaking from the tubing through the leakage hole into the annulus. The process can be divided into the following steps, detailed below:

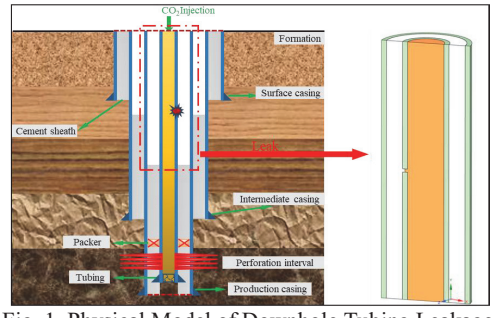

Fig. 1. Physical Model of Downhole Tubing Leakage

2.1.1 *Initial Jet*

During the initial stage of CO_2 leakage, liquid CO_2 jets out from the leakage hole in the downhole tubing, forming a laminar jet. At this time, the jet front is very distinct, exhibiting regular and stable flow behavior. The initial speed and pressure of the jet are primarily driven by the internal pressure of the tubing, and the flow near the leakage hole exhibits characteristics of laminar flow.

2.1.2 *Jet Development*

As the jet expands outward, at a certain distance from the leakage hole, the jet front begins to break up and form disturbance waves. These disturbance waves increase the instability of the flow and generate vortex structures within the jet, making the jet structure more complex.

2.1.3 *Turbulent Development of Jet Head*

As the jet continues to develop, when the jet reaches a further distance from the leakage hole, the initial laminar portion gradually transitions to a turbulent state. At this distance, the flow becomes unstable, and the turbulent development of the jet head accelerates, making the transitional region more pronounced. Here, the contrast between the laminar and turbulent regions is evident, resulting in more complex flow behavior.

2.1.4 *Jet Front Impacting Casing Wall*

Further development of the jet leads to the front impacting the casing wall. At this point, the jet breaks up, and the laminar portion shortens, making the flow disordered and with turbulence becoming dominant. In this region, the jet speed increases from zero to the main flow speed, marking a significant development process. Interaction with the wall further enhances flow instability.

2.1.5 *Formation of Compressed Mixing Zone Along Casing Wall*

When CO_2 encounters obstacles, the flow decelerates and reverses. The fluid separates from the wall, forming a complex flow structure. This complex flow results in the formation of a highly compressed mixing zone in the local area. This mixing zone displays high turbulence characteristics and vortex structures, making the jet flow in the local area more complex and unstable.

2.2 *Governing equation and phase change model*

The multiphase flow model in this study utilizes the mixture model. We found that interphase slip had no significant effect on the transient depressurization characteristics of CO_2. Therefore, interphase slip was neglected in this study. By eliminating the slip terms, the control equations for the mixture model are simplified as follows:

$$\frac{\partial \rho_m}{\partial t} + \nabla \cdot (\rho_m \mathbf{v}_m) = 0 \tag{1}$$

$$\frac{\partial}{\partial t}(\alpha_q \rho_q) + \nabla \cdot (\alpha_q \rho_q \mathbf{v}_m) = 0 \tag{2}$$

$$\frac{\partial}{\partial t}(\rho_m \mathbf{v}_m) + \nabla \cdot (\rho_m \mathbf{v}_m \mathbf{v}_m) = -\nabla p + \nabla \cdot (\mu_m (\nabla \mathbf{v}_m + \nabla \mathbf{v}_m^T)) + \mathbf{F} \quad (3)$$

$$\frac{\partial}{\partial t}(\rho_m E_m) + \nabla \cdot (\mathbf{v}_m (\rho_m E_m + p_m)) = \nabla \cdot (k_m \nabla T) + \Phi_m \quad (4)$$

In this context, Eq. (1) represents the continuity equation for the mixture, Eq. (2) represents the continuity equation for each phase, Eq. (3) represents the momentum equation for the mixture, and Eq. (4) represents the energy equation for the mixture. Here, ρ_m denotes the density of the mixture; t denotes time; $\mathbf{v}_m$ denotes the velocity vector of the mixture; α_q denotes the volume fraction of the q-th phase; ρ_q denotes the density of the q-th phase; p denotes the pressure of the mixture; μ_m denotes the dynamic viscosity of the mixture; $\mathbf{F}$ denotes the body force; E_m denotes the total energy of the mixture; p_m denotes the pressure of the mixture; k_m denotes the thermal conductivity of the mixture; T denotes the temperature; and Φ_m denotes the viscous dissipation term.

During the rapid depressurization of CO_2 leakage, the primary driving force for phase change is the change in pressure. The Zwart-Gerber-Belamri cavitation phase change model is employed to simulate this process. The Zwart-Gerber-Belamri model focuses on cavitation phenomena caused by local pressure dropping below the vapor pressure. The expression is as follows:

$$\frac{\partial \alpha_v}{\partial t} + \mathbf{v}_m \cdot \nabla \alpha_v = \frac{1}{\rho_l}(R_e - R_c) \quad (5)$$

$$R_e = F_e \sqrt{\frac{2}{3}\frac{p_v - p}{\rho_l}}(1-\alpha_v)^n \quad (6)$$

$$R_c = F_c \sqrt{\frac{2}{3}\frac{p - p_v}{\rho_l}}\alpha_v^m \quad (7)$$

$$R = \left(\frac{3\alpha_v}{4\pi n_0}\right)^{\frac{1}{3}} \quad (8)$$

In this context, Eq. (5) represents the mass transfer equation, Eq. (6) and Eq. (7) respectively represent the evaporation rate and condensation rate, and Eq. (8) represents the bubble radius. Here, α_v denotes the volume fraction of the vapor phase; ρ_l denotes the liquid density; R_e represents the evaporation rate (mass generation term); R_c denotes the condensation rate (mass disappearance term); p_v denotes the vapor pressure (saturated vapor pressure); p denotes the local pressure; R denotes the bubble radius; n_0 denotes the initial bubble density (number of bubbles per unit volume); and n and m denote empirical exponents.

2.3 *Turbulence model*

To close the governing equations, it is necessary to consider the turbulence model for the CO_2 leakage and confined jet. Here, the Large Eddy Simulation (LES) model (Wang and Zang et al. 2022) is utilized. This model directly simulates large-scale turbulent motions in the fluid, while small-scale turbulence is handled using a subgrid-scale model. The LES model simulates turbulent flow by solving the filtered Navier-Stokes equations.

2.4 *Thermophysical properties*

In the numerical simulation of the high-pressure CO_2 rapid depressurization process, the accurate assessment of the thermophysical properties of CO_2 directly affects the prediction accuracy of transient flow behavior. In this study, the thermophysical properties of liquid and gaseous CO_2 were fitted using the least squares method based on the NIST database. The fitted formulas for density, specific heat capacity, speed of sound, dynamic viscosity, and thermal conductivity were compiled into a User-Defined Function (UDF) and embedded into the Fluent computational model. In this study, the air in the annulus was treated as an ideal gas.

2.5 *CFD model and boundary condition*

This paper investigates the depressurization and expansion flow of high-pressure CO_2 leaking

from a wellbore into the annular space through a small orifice. Considering that the geometric model is symmetric about the xz-plane and xy-plane, to improve computational efficiency, a quarter model was selected for the simulation. The geometric model is shown in Figure 2. The wellbore cross-section is set as the pressure inlet condition, the annular cross-section is set as the pressure outlet condition, and the xz-plane and the xy-plane of the model are set as symmetric boundary conditions. Due to the brief duration of the instantaneous leakage, all other wall surfaces are set as adiabatic walls.

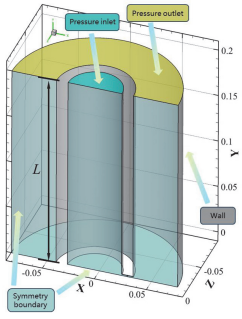

Fig. 2. Geometric Model

In this simulation, a pressure-based transient solver is employed to solve the multiphase flow equations, with a time step set to 1E-6. The Coupled scheme is used for pressure-velocity coupling, along with coupling for the multiphase volume fractions. The "Least Squares Cell Based" discretization method is used for gradient variables, and the "PRESTO!" method is used for pressure variables. The volume fractions are discretized using the "QUICK" scheme, while other variables are discretized using the "Second Order Upwind" scheme.

2.6 *Grid independence*

The computational domain consists of a high-pressure CO_2 wellbore and an external annular air region, connected by a leakage orifice. The outer diameter of the wellbore is 73.0 mm, with a wall thickness of 5.51 mm. The inner diameter of the production casing is 160 mm. The wellbore has a circular orifice serving as the leakage point. The study investigates the effects of leakage orifice diameters of 1.0 mm on the flow field structure and flow characteristics. The model length is 200 mm. The geometric model is meshed using Fluent meshing, as shown in Figure 3. The mesh is refined around the leakage orifice, with a refined mesh size of 0.5 mm and a mesh size of 4.0 mm in other regions. The quarter model consists of approximately 1.42 million cells.

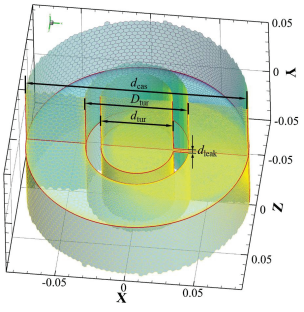

Fig. 3. Mesh Generation

3 Results and discussion

This paper focuses on the analysis of the flow field parameter variations in the xoz cross-section of a leakage hole at different time intervals (0.16 ms, 0.50 ms, 0.70 ms, and 1.00 ms). The initial conditions include an initial pressure of 10 MPa, an initial temperature field of 300 K, and a leakage orifice diameter of 1.0 mm.

In Figure 4, we illustrate the variation of instantaneous temperature during the leakage process. The figure demonstrates that, during the leakage process, due to the Joule-Thomson effect and pressure drop-induced phase change, the temperature in the jet core region decreases, with the lowest temperature reaching 280 K, resulting in an overall temperature drop of up to 20 ℃. At 1.00 ms, transient leakage stabilizes, and localized low-temperature CO_2 splashing regions can be observed on the casing wall.

Figure 5 shows the temperature variation along the axis of the leakage hole during transient leakage, with an initial temperature of 26.85 ℃ (300 K). Near the leakage hole, the fluid temperature increases as the fluid undergoes compression at the leakage hole, releasing heat and causing the temperature to rise in the vicinity.

Conversely, as the fluid passes through the leakage hole, it undergoes decompression and expansion, leading to phase change and a corresponding decrease in temperature. As the leakage progresses, the temperature near the casing wall further decreases, reaching a minimum temperature of 8 ℃.

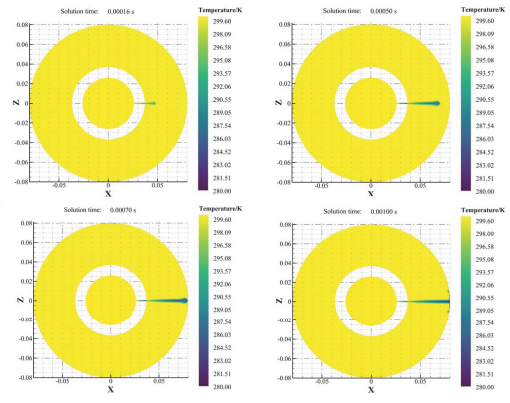

Fig. 4. Temperature variation over time on the xz cross-section

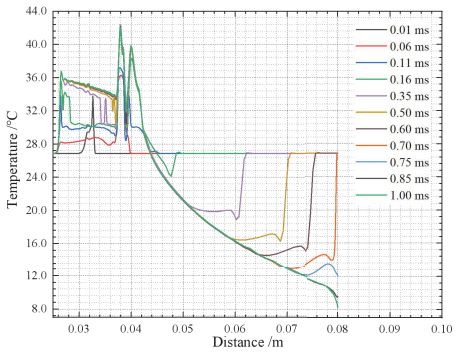

Fig. 5. Temperature variation along the axis of the leakage hole

In Figure 6, we illustrate the variation of instantaneous velocity during the leakage process. From the figures, it can be observed that fluid velocity is relatively low in the leakage hole region due to the throttling effect. As the fluid flows through the leakage hole and progresses, the maximum velocity region at each moment is concentrated near the leakage hole. This is primarily because the decompression and expansion of the fluid result in a high velocity in the jet core region. On the casing wall, the fluid velocity is the lowest due to the obstruction effect of the wall.

Figure 7 shows the velocity variation along the axis of the leakage hole during transient leakage. The figure reveals that the maximum velocity in the overall flow reaches around 200 m/s in the leakage hole region, which is within the subsonic range. As the fluid flows through the leakage hole, the velocity reaches a maximum of approximately 280 m/s. On the casing wall, the fluid velocity drops sharply, with the maximum velocity decreasing to around 100 m/s.

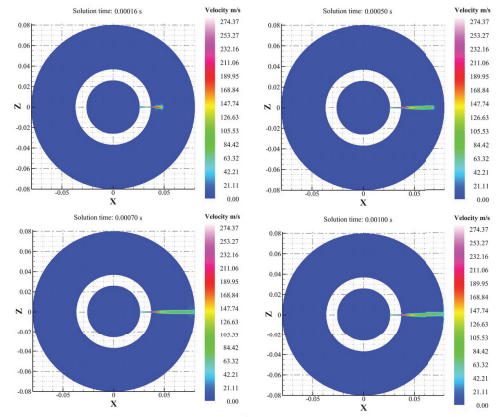

Fig. 6. Velocity variation over time on the xz cross-section

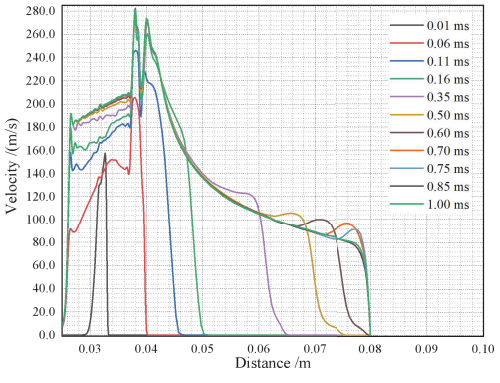

Fig. 7. Velocity variation along the axis of the leakage hole

In Figures 8 and 9, we illustrate the instantaneous changes in vorticity and pressure during leakage. From the figures, it can be

observed that during the initial stage of leakage, the vorticity and pressure change rapidly due to the decompression and expansion of the fluid passing through the leakage hole. As the pressure drops rapidly, the area forming vortices gradually increases. As the leakage process continues, the rate of pressure drop slows down, reaching a relatively stable stage, during which the vorticity changes also tend to stabilize.

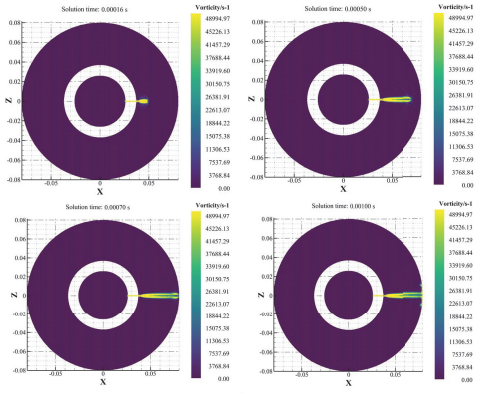

Fig. 8. Vorticity variation over time on the xz cross-section

Figure 9 shows the variation of pressure along the axis of the leakage hole during transient leakage. The figure indicates that due to the throttling effect of the small leakage hole, the high-pressure fluid causes noticeable compression in the leakage hole region, resulting in a pressure increase to approximately 11.5 MPa. In the stable leakage stage, both the pressure and vorticity near the leakage hole tend to stabilize. The vorticity changes are mainly concentrated in the vortex region near the leakage hole and the casing wall, while the pressure exhibits a downward trend throughout the leakage region. Together, these observations highlight that during the initial phase of leakage, decompression and fluid expansion play significant roles in the rapid changes of vorticity and pressure. Subsequently, as the process stabilizes, the system reaches a steady state where these quantities become stable, providing insights into the fluid dynamics of the leakage process.

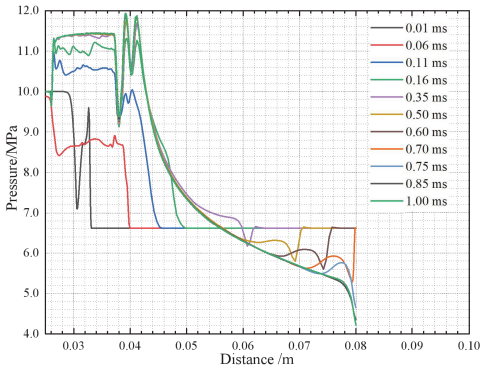

Fig. 9. Pressure variation along the axis of the leakage hole

4 Conclusion Prospects

4.1 *Conclusion*

(1) During the leakage process, influenced by the Joule-Thomson effect and decompression phase transition, the temperature in the jet core region decreases, reaching as low as 280 K with an overall temperature drop of up to 20°C. Near the leakage hole, the fluid temperature initially increases due to compression, then decreases due to decompression and expansion, reaching a minimum temperature of 8°C.

(2) The fluid velocity is lowest at the leakage hole due to throttling effects and increases as it flows through the leakage hole, with the maximum velocity reaching approximately 280 m/s in the jet core region due to decompression and expansion. The velocity decreases significantly near the casing wall, with the lowest value around 100 m/s.

(3) In the initial stage of leakage, vorticity and pressure change rapidly due to fluid decompression and expansion. As pressure drops, the vortex region enlarges. Over time, the rate of pressure drop slows and stabilizes, with vorticity changes also stabilizing. The pressure in the leakage hole region increases slightly to around 11.5 MPa due to high-pressure fluid compression.

(4) Upon reaching a stable leakage stage, both pressure and vorticity near the leakage hole stabilize. Vorticity changes are focused in the vortex region near the leakage hole and casing

wall, while pressure tends to decrease throughout the leakage area.

4.2 *Prospects*

(1) Based on the CFD flow simulation results obtained in this study, future work will use *LMS Virtual.Lab* to establish a distributed quadrupole acoustic source model based on aeroacoustics. This approach will enable us to obtain the characteristics of acoustic sources under different tubing pressures and leakage hole diameters. The insights from these flow-acoustic simulations can provide detection basis for the early discovery of downhole tubing leakage in CO_2 injection wells based on acoustic principles, thereby further improving the safety and reliability of CCS projects.

(2) Future research should focus on experimental validation to improve the accuracy and reliability of the CFD model and flow-acoustic simulation results. By setting up controlled experiments to measure temperature, pressure, flow velocity, and acoustic source parameters under different leakage scenarios, we can better validate the simulation results and further optimize the model.

References

Chen, S., R. Gojon, and M. Mihaescu.(2021). Flow and aeroacoustic attributes of highly-heated transitional rectangular supersonic jets. *Aerospace Science and Technology*, **114**: 106747.

Cheng, L., K. Zhang, B. Luo, L. Deng, and H. Cheng.(2024). A new numerical model of gas leakage noise from elliptical sealing defects in pipelines. *Applied Acoustics*, **217**: 109829.

Elshahomi, A., C. Lu, G. Michal, X. Liu, A. Godbole, and P. Venton.(2015). Decompression wave speed in CO_2 mixtures: CFD modelling with the GERG-2008 equation of state. *Applied Energy*, **140**: 20-32.

Flechas, T., D. M. Laboureur, and C. J. Glover.(2020). A 2-D CFD model for the decompression of carbon dioxide pipelines using the Peng-Robinson and the Span-Wagner equation of state. *Process Safety and Environmental Protection*, **140**: 299-313.

Liu, B., X. Liu, C. Lu, A. Godbole, G. Michal, and A. K. Tieu.(2018). A CFD decompression model for CO_2 mixture and the influence of non-equilibrium phase transition. *Applied Energy*, **227**: 516-24.

Liu, X., A. Godbole, C. Lu, G. Michal, and P. Venton.(2014). Source strength and dispersion of CO_2 releases from high-pressure pipelines: CFD model using real gas equation of state. *Applied Energy*, **126**: 56-68.

Luo, Z., P. Wu, H. Wen, Y. Wang, C. Liu, X. Du, and L. Liu.(2024). Effect of source strength on the simulation of jet dispersion and hazard distances during accidental release of liquid CO_2. *Process Safety and Environmental Protection*, **183**: 1152-69.

Peng, H., H. Lu, Z. Xu, D. Xi, and G. Qin.(2024). Failure mechanism of carbon dioxide transport infrastructure: A comprehensive review. *International Journal of Greenhouse Gas Control*, **135**: 104144.

Teng, L., X. Liu, J. Bian, Y. Li, and C. Lu.(2020). A homogeneous relaxation model for multi-phase CO_2 jets following the release of supercritical CO_2 pipelines. *Journal of Natural Gas Science and Engineering*, **84**: 103609.

Wang, H., J. Zang, J. Wang, and Y. Huang.(2022). Large eddy simulation of the heat transfer and unsteady pulsation of supercritical carbon dioxide in a square subchannel. *International Journal of Thermal Sciences*, **172**: 107377.

Wei, X. F., R. Mariani, L. P. Chua, H. D. Lim, Z. B. Lu, Y. D. Cui, and T. H. New.(2019). Mitigation of under-expanded supersonic jet noise through stepped nozzles. *Journal of Sound and Vibration*, **459**: 114875.

Xi, D., H. Lu, Y. Fu, S. Dong, X. Jiang, and J. Matthews.(2023). Carbon dioxide pipelines: A statistical analysis of historical accidents. *Journal of Loss Prevention in the Process Industries*, **84**: 105129.

Zhang, J., Z. Lian, Z. Zhou, M. Xiong, M. Lian, and J. Zheng.(2021). Acoustic method of high-pressure natural gas pipelines leakage detection: Numerical and applications. *International Journal of Pressure Vessels and Piping*, **194**: 104540.

Zhu, M., C. Pérez Arroyo, A. Fosso Pouangué, M. Sanjosé, and S. Moreau.(2018). Isothermal and heated subsonic jet noise using large eddy simulations on unstructured grids. *Computers & Fluids*, **171**: 166-92.